IEEE Access
Multidisciplinary | Rapid Review | Open Access Journal

Received September 10, 2020, accepted September 14, 2020, date of publication September 21, 2020,
date of current version October 1, 2020.

Digital Object Identifier 10.1109/ACCESS.2020.3025560

Research on Passing Ability and Climbing Performance of Pipeline Plugging Robots in Curved Pipelines

HONGWEI YAN, LU WANG, PENGCHENG LI, ZHIJIAN WANG, XIONG YANG, AND XIANGRONG HOU

School of Mechanical Engineering, North University of China, Taiyuan 030051, China

Corresponding author: Hongwei Yan (aweigeyan@nuc.edu.cn)

This work was supported in part by the Research Project through the Shanxi Scholarship Council of China under Grant 2020-110, in part by the National Natural Science Foundation under Grant 51905496, and in part by the Shanxi Province Key Technologies Research and Development Program of China under Grant 201603D321117.

ABSTRACT To repair leaking pipelines for oil, natural gas and other dangerous media, a kind of pipeline sealing robot is proposed. The device is mainly divided into a robot drive unit, connection unit, and blocking unit. The robot drive unit is used to pull the blocking unit, allowing it to move in the pipeline. The connection unit is used to connect the robot drive unit and the blocking unit. The blocking unit is used to complete the repair at the leakage point. When the robot operates, the drive unit drags the blocking device to the pipeline leakage location, and the front camera can detect the size and shape of the leakage hole. The sealing unit is located at the leakage point, an airbag is inflated, and the adhesive in it is used to seal and repair the leak. Two performance indices (climbing performance and curve passing performance) are evaluated when the robot drive unit is walking. A 3D model of the robot is established, and the performance index of the robot is simulated and analyzed using virtual prototype technology. An experimental platform is built for verification. The conclusions are as follows: (1) A spring with a 13 N/mm rigidity yielded the best performance, and the robot could crawl up a 37° slope. (2) When the deflection angle of the driving wheel was set to 30°, the robot could smoothly pass a bend with a radius of curvature of 500 mm. Thus, the robot performance met the design requirements.

INDEX TERMS Pipeline plugging robots, passing ability, climbing performance, ADAMS.

I. INTRODUCTION

With the widespread application of fluid energy [1], such as oil and natural gas [2], pipeline transportation has become an increasingly important energy transportation method [3]. In addition, pipelines also play an important role in urban water transport [4]. With the large-scale development of pipeline engineering [5], the service lives of pipelines have been prolonged [6], and accidents caused by human damage, media corrosion, and other factors leading to pipeline leakage have increased annually [7]. Once leakage occurs, a large-scale dangerous chemical spill can easily occur [8], which not only causes property loss, but also significantly threatens human lives and safety [9].

The associate editor coordinating the review of this manuscript and approving it for publication was Hiram Ponce.

Traditional pipeline leak detection uses a random extraction method, which has a high degree of uncertainty [10], as there are toxic and harmful gases in the pipeline [11]. It is difficult to manually complete pipeline detection and plugging repair tasks [12]. Thus, pipeline robots are increasingly favored by scientific researchers [13], engineers, and technical personnel. Many scholars have also begun to study suitable plugging repair methods for different pipeline leakage scenarios to repair pipelines quickly, efficiently, and safely [14].

Existing pipeline robots are classified as fluid-driven, wheeled, crawler-type, driving-type, peristaltic, and spiral-driven types according to their motion modes and mechanical structures. A pipeline inspection gauge (PIG) is a kind of driven robot without its own power input [15]. Its power is derived from the pressure difference of the fluid medium

TABLE 1. Advantages and disadvantages of different driving methods.

Motion modes	Fluid-driven	Wheeled	Crawler-type	Driving-type	Peristaltic	Spiral-driven
Advantages	Simple structure, high endurance	Simple structure, easy to control, large driving force	Strong barrier-crossing ability, good motion performance	Large driving force, can complete complex movements in tube	Simple structure and light weight	Simple mechanism large driving force easy to control, speed, large load capacity high positioning accuracy
Disadvantages	Poor controllability, poor ability to cross obstacles	Unstable energy supply , small battery capacity slips easily	Complex mechanism, difficult to control, poor flexibility	Complicated drive system, high cost difficult to control speed	Only suitable for pipes with small diameters, unable to pass through bent and inclined pipes	Weak ability to cross obstacles

at both ends of the equipment, and it moves against friction [16]. PIGs have simple structures and high endurance properties [17]. However, they have the disadvantages of poor controllability and weak obstacle surmounting abilities [18]. Ho Moon Kim *et al.* [19], a scholar at Sungkyunkwan University in South Korea, proposed a wheeled in-tube robot based on a multi-axis differential gear mechanism, called MRINSPECT VII. This robot had a simple structure and was easy to control, but the power source capacity was small and the robot could easily slip. Nagase *et al.* [20], a scholar at Ryukoku University in Japan developed a cylindrical elastic crawler robot for pipeline inspection [21]. This extremely simple structure had a unique steering mechanism, which enabled the robot to perform well in vertical pipelines, curved corners, and uneven narrow pipeline areas [22]. The Andreas Zagler team at the Munich University of Technology in Germany developed a walking pipeline robot named MORITZ. This robot could complete complex movements, but its body drive system was too complicated, the cost was high, and the speed was difficult to control [23]. Yuki *et al.* [24], a scholar from Chuo University of Japan designed a peristaltic robot for underwater pipeline inspection [25] and studied its control system for contraction forces [26]. Kamata *et al.* [27] developed a pneumatic peristaltic pipe robot for long-distance pipe inspection, but this robot could not pass elbows or straight tubes with inclination angles. By comparing the advantages and disadvantages of the different movement methods shown in Table 1 and considering the complex working environment of the plugging and repairing robot designed in this study, we selected the spiral driven type robot [28].

At present, few scholars have simultaneously studied pipeline inspection and plugging repair. Based on existing conditions, a pipe sealing robot was developed in this study that can complete the inspection and repair of small holes, cracks, and other defects in pipes with inner diameters of 200 mm. The device can pass through a curved pipe smoothly because the walking unit of the device contains a spring, and the expansion and contraction of the spring ensures that the wheels are in close contact with the pipe wall. The climbing performance and bendability of the robot are primarily examined in this article. The rationality and superiority of the robot design was verified.

II. STRUCTURAL DESIGN OF PLUGGING ROBOT IN PIPELINE

The designed robot mainly operates in a pipeline with a dangerous medium such as oil and gas, and its working environment is complex. Therefore, the performance requirements of the robot are relatively high [29], mainly including climbing and curve passing [30].

A. DESIGN REQUIREMENTS OF PLUGGING ROBOT IN PIPELINE

The in-pipe plugging robot designed in this study mainly performs emergency treatment and disposal of the leaking pipeline to complete the repairing function. The plugging robot in the pipeline mainly includes a robot drive unit and a plugging unit. The technical requirements that the overall system must meet when completing the structural design are shown in Table 2.

TABLE 2. Technical requirements for plugging robots in pipelines.

Project	Index
Pipe Diameter Range	180–210 mm
Slope Climbing Capability	Not less than 30°
Driving Speed in Straight Tube	$v \geq 3$ m/min
Tractive Force	$F \geq 30$ N
Radius of Curvature	$\rho \geq 500$ mm
Total Length of Plugging Robot in Pipeline	$L \leq 600$ mm
Total Weight of Plugging Robot in Pipeline	$m \leq 10$ kg
Effective Plugging Pressure	1 MPa

B. OVERALL STRUCTURE OF PLUGGING ROBOT IN PIPELINE

To increase the robot's ability to adapt to bends, the overall structure is designed in a modular series. This mainly includes a robot drive unit, a connection unit, and a plugging unit. The overall structure is shown in Figure 1. A robot drive unit can connect several plugging units in series through the connection unit to realize the multi-point discrete plugging of a leaking pipeline, thereby increasing the plugging area and enhancing the overall plugging reliability.

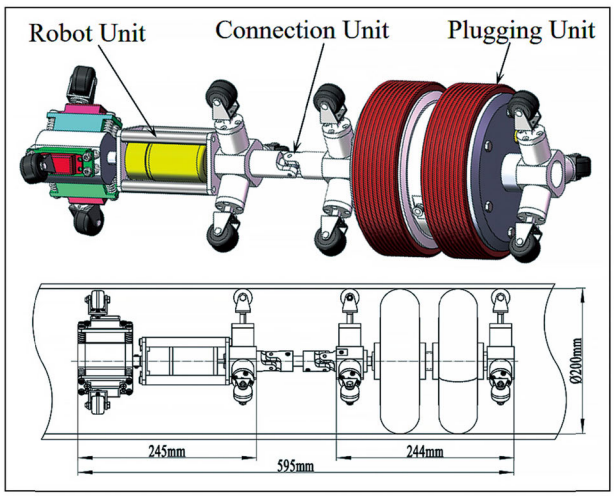

FIGURE 1. Overall structure of the plugging robot in the pipeline.

1) ROBOT DRIVE UNIT DESIGN

For a plugging robot in a pipeline, the robot drive unit mainly provides power for operation within the pipeline. Based on the design requirements, the robot must operate smoothly in a complex pipeline environment, which creates higher requirements for the robot drive unit, such as sufficient traction, strong environmental adaptability, and suitable driving speeds. Therefore, a reasonable design of the robot drive unit is key for improving the performance of the plugging robot in the pipeline, and it is also the focus of the entire device design.

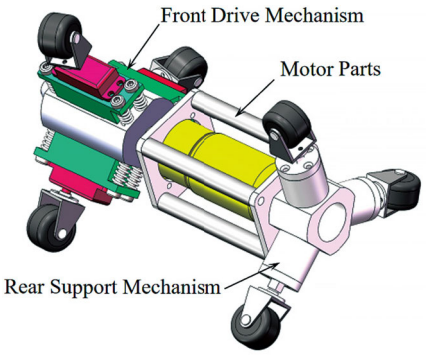

FIGURE 2. Robot drive unit of the structure diagram.

The robot drive unit includes a front drive mechanism, a motor, and a rear support mechanism. The overall structure is shown in Figure 2. The front driving mechanism adopts a spiral-driving walking method, and the rear supporting part adopts a spring supporting method.

a: STRUCTURAL DESIGN OF FRONT DRIVE MECHANISM

The servos can control the deflection of the wheel frame, thereby controlling the deflection angle of the driving wheel. The front drive mechanism is mainly composed of a driving frame, steering gear cover, steering gear, driving wheel, wheel frame, and spring. It is the power output component of the entire robot, and it drives the steering gear, steering gear shield, and wheel frame to perform circular rotation. The driving frame is the supporting structure of the overall driving mechanism. The steering gear cover is mainly used to protect the steering gear and prevent wear and damage due to the direct contact between the steering gear and the driving frame. The steering gear is installed inside the steering gear protective cover, which can ensure the rigid connection of the driving wheel and the steering gear protective cover. The steering gear is connected to the wheel frame, which can control the deflection of the wheel frame and thus the deflection angle of the driving wheel. The structure of the front drive mechanism directly affects the robot's capabilities, such as its traction and bendability. The steering gear is installed inside the steering gear protective cover, which can ensure the rigid connection of the driving wheel and the steering gear protective cover. The front drive mechanism adopts a spiral drive walking mode, and the structure diagram is shown in Figure 3. The spring is used to assist the robot to adapt to pipes of different pipe diameters. The designed front drive mechanism can adapt to a pipe diameter range of 180 – 210 mm.

b: MOTOR COMPONENT

The motor component is mainly composed of the connecting front plate, connecting rear plate, connecting pipe, and motor. The front and back plates are fastened by screws to the

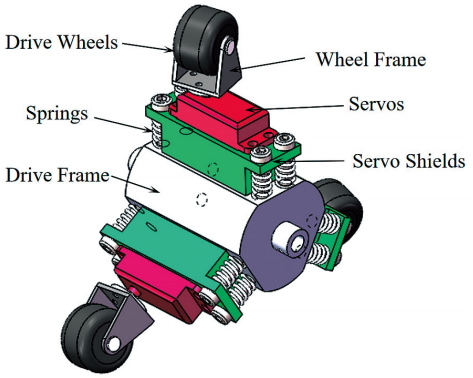

FIGURE 3. Structural diagram of the front drive mechanism.

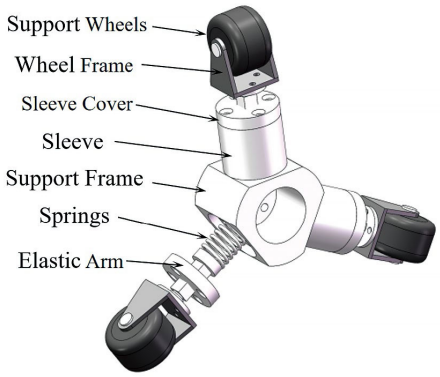

FIGURE 5. Structure of the rear support mechanism.

connecting pipe, which supports and protects the motor, and the entire unit can also provide an explosion-proof function.

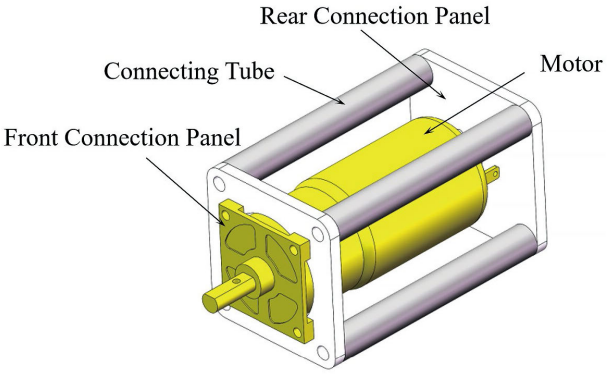

FIGURE 4. Structure of the motor.

The motor is used as the power input of the entire robot. Considering that the plugging device must be connected, and a certain load capacity is required, a 775 DC geared motor was pre-selected. The structure of the motor is shown in Figure 4.

c: STRUCTURAL DESIGN OF REAR SUPPORT MECHANISM

The rear support mechanism is composed of an elastic arm, spring, support frame, sleeve, sleeve cover, wheel frame, and support wheel. During operation, it cooperates with the front drive mechanism to support and adapt to different pipeline environments. The back-support mechanism uses a spring support with a simple structure and strong applicability. The overall structure is shown in Figure 5.

2) CONNECTION UNIT DESIGN

The function of the connection unit is to flexibly connect the robot drive unit and the plugging unit so that the robot can smoothly pass through the turning point of the pipeline. Meanwhile, the connection unit must ensure that during the turning of the entire robot, problems such as interference of various parts cannot occur. After screening and comparison, the connection scheme selected was a universal connection. The joint mechanism of the connecting unit does not involve relative rotation, so the number of degrees of freedom of the joint mechanism of the connection unit is 2.

3) PLUGGING UNIT DESIGN

The plugging unit includes the rear support mechanism and the plugging mechanism, which are the key operating parts of the robot when performing the plugging task. It mainly aims to repair leaks, such as small holes or cracks, that may occur during long-term service of a pipeline. The overall structure of the plugging unit is shown in Figure 6. The back-support mechanism is the same as the back-support mechanism of the robot drive unit. The plugging mechanism uses a double airbag plugging method, which has the advantages of a wide plugging area, strong adaptability, and a fast response speed.

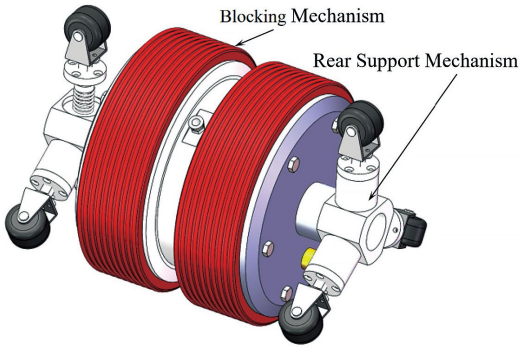

FIGURE 6. Schematic diagram of the overall structure of the plugging unit.

The plugging mechanism is composed of a solenoid valve, end cap, quick-plug inflation interface, support ring, plugging airbag, and fixed ring. The overall structure is shown in Figure 7. The end cap is provided with a diversion port and a quick-plug inflation interface, and a solenoid valve is connected to the diversion port. The role of the solenoid valve is to control the opening and closing of the diversion port. Controlling the solenoid valve to open the diversion port can reduce the resistance of the fluid medium to the blocking unit when the robot drives in the liquid pipe. The plugging airbag is sleeved on a fixing ring, the plugging airbag equipped

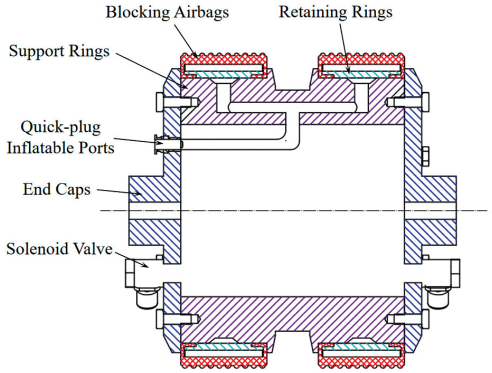

FIGURE 7. Schematic diagram of the overall structure of the plugging mechanism.

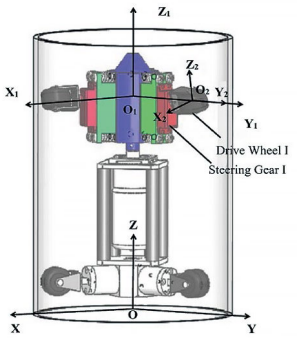

FIGURE 8. Schematic diagram of the robot driving in a straight pipe.

with the fixing ring is installed on the support ring, and the end cap is tightly closed to complete the installation of the plugging airbag. At the same time, the robot is equipped with an automatic inflation device, which is connected to a rapid inflation interface. When blocking is required, the host computer controls the start button to complete the inflation and blocking. When a single point leak occurs in the pipeline, a robot can be used to plug it, and the sealing air bag can be inflated to fully fit the leakage point of the pipeline wall for plugging. At the same time, the solenoid valve opens the diversion port, so that the fluid in the pipeline can continue to flow through the diversion port. When the pipeline leak or damage is severe, two sets of robots and plugging devices are operated simultaneously. The cover layers of the two sets of plugging airbags are pressed on both ends of the pipe wall rupture, so that the fluid medium between the two sets of plugging devices forms an isolated space, and then the broken pipe is cut for replacement.

III. KINEMATIC ANALYSIS OF PLUGGING ROBOT IN PIPELINE

The analysis of the motion characteristics of the pipeline robot involves two tasks: the first is the representation of the motion equation of the pipeline robot in the process of walking, i.e., forward kinematic analysis, and the second is the solution of the motion equation of pipeline robot, i.e., inverse kinematic analysis. In this paper, the analysis of the motion characteristics of the pipeline robot belongs to the first kind of problem. The Denavit–Hartenberg D-H method is used [31], which is a coordinate conversion method. It mainly analyzes the motion characteristics of the pipeline robot when walking in two different pipelines: straight and curved [32].

A. ANALYSIS OF MOTION CHARACTERISTICS OF PLUGGING ROBOT IN STRAIGHT PIPELINE

Straight pipes are the main components of pipelines, and they are also the most basic type of oil and gas pipeline [33]. The analysis of the kinematics of a robot in a straight pipe is the most basic and necessary task. The driving state of the proposed robot in a straight pipe is shown in Figure 8. The influence of the robot's own weight on the deviation of its central trajectory is ignored, and it is assumed that the contact statuses of all the wheels and the pipe wall are the same. The following parameters are defined:

$\boldsymbol{R}$ is the radius of the straight pipe, $\boldsymbol{r}$ is the radius of the inner plugging robot wheel, α ' is the speed of the drive frame (motor speed), and θ is the deflection angle of the drive wheel.

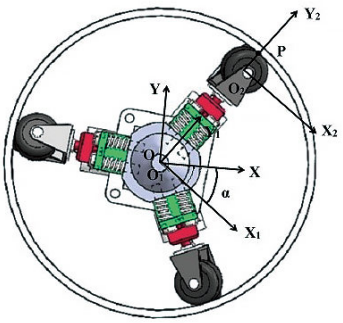

FIGURE 9. Rotation angle representation of the drive frame.

To study the motion state of the robot in a straight pipe, a coordinate system was established in the driving schematic diagram shown in Figure 8. {O} is the global coordinate system, which is established on the ground, and the central axis of the robot is the Z axis in {O}. $\{O_1\}$ is the dynamic coordinate system on the robot drive frame. Its origin is the intersection of the plane formed by the central axis of the pipe and the centerline of the three servo shafts in the drive frame. The origin is represented in {O} as $(0\ 0\ z)^T$. The Z_1 axis is collinear with the Z axis in the global coordinates, and the Y_1 axis is collinear with the centerline of the output shaft of servo I. The X_1Y_1 plane in {O} rotates around the Z axis in {O}, and the rotation angle is denoted as α (the angle between the X_1 and X axes is denoted as α). As shown in Figure 9, α ' can represent the rotation speed of the driving frame, that is, the rotation speed of the motor. $\{O_2\}$ is the dynamic coordinate system on the geometric center of the driving wheel of the robot, and its origin is expressed as $(0\ R\text{-}r\ 0)^T$ in $\{O_1\}$. Its Y_2 axis is collinear with the Y_1 axis

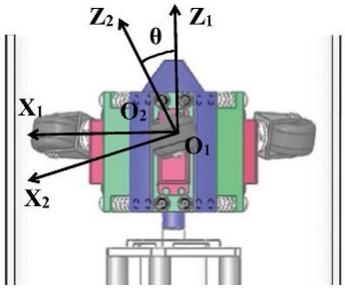

FIGURE 10. Driving wheel deflection angle representation.

of $\{O_1\}$, and the Z_2 axis is perpendicular to the radial center plane of driving wheel I. The deflection angle of the Z_2 axis in $\{O_2\}$ relative to the Z_1 axis of $\{O_1\}$ is θ (the deflection angle of the driving wheel of the robot), as shown in Figure 10.

Different reference coordinate systems are set in different regions based on the movement of the robot, and each reference coordinate system can be converted to the others. The coordinate conversion method is used to convert each reference coordinate system into a matrix coordinate system. The specific expression is as follows:

$$ {}^0_1T = \begin{bmatrix} \cos\alpha & -\sin\alpha & 0 & 0 \\ \sin\alpha & \cos\alpha & 0 & 0 \\ 0 & 0 & 1 & z \\ 0 & 0 & 0 & 1 \end{bmatrix} \tag{1} $$

$$ {}^1_2T = \begin{bmatrix} \cos\theta & 0 & \sin\theta & 0 \\ 0 & 1 & 0 & R-r \\ -\sin\theta & 0 & \cos\theta & 0 \\ 0 & 0 & 0 & 1 \end{bmatrix} \tag{2} $$

The contact between the driving wheel and the inner wall of the pipe is assumed to be a point contact, and the contact point between driving wheel I and the inner wall of the pipe is set to $\boldsymbol{P}$. The point $\boldsymbol{P}$ in the $\{O_2\}$ dynamic coordinate system is expressed as follows:

$$ {}^2P = (0 \quad r \quad 0)^T \tag{3} $$

According to the coordinate transformation relationship, the contact point P is expressed in $\{O\}$ as follows:

$$ \begin{bmatrix} {}^0P \\ \hline 1 \end{bmatrix} = {}^0_1T\,{}^1_2T \begin{bmatrix} {}^2P \\ \hline 1 \end{bmatrix} \tag{4} $$

Substituting the above formulas into Equation (4) gives the following:

$$ {}^0P = \begin{bmatrix} -R\sin\alpha \\ R\cos\alpha \\ z \end{bmatrix} \tag{5} $$

Assuming that the driving wheel of the robot does not slide axially during the spiral advancing process, the speed projection of driving wheel I in the Z_2 axis direction is 0, which is expressed as follows:

$$ {}^0P' \cdot {}^0e_{Z_2} = 0 \tag{6} $$

The direction vector of the Z_2 axis in $\{O_2\}$ is expressed as follows:

$$ {}^2e_{Z2} = \begin{bmatrix} 0 & 0 & 1 \end{bmatrix}^T \tag{7} $$

The direction vector of the Z_2 axis in $\{O_2\}$ is expressed in $\{O\}$ as follows:

$$ {}^0e_{Z_2} = {}^0_1R^1_2R\,{}^2e_{Z_2} \tag{8} $$

In these equations, ${}^0_1R$ and ${}^1_2R$ are expressed as follows:

$$ {}^0_1R = \begin{bmatrix} \cos\alpha & -\sin\alpha & 0 \\ \sin\alpha & \cos\alpha & 0 \\ 0 & 0 & 1 \end{bmatrix} \tag{9} $$

$$ {}^1_2R = \begin{bmatrix} \cos\theta & 0 & \sin\theta \\ 0 & 1 & 0 \\ -\sin\theta & 0 & \cos\theta \end{bmatrix} \tag{10} $$

Substituting Equations (9) and (10) into Equation (8) gives the following:

$$ {}^0e_{Z_2} = \begin{bmatrix} \cos\alpha\sin\theta \\ \sin\alpha\sin\theta \\ \cos\theta \end{bmatrix} \tag{11} $$

which in turn yields

$$ z' = R\alpha'\tan\theta \tag{12} $$

The analysis shows that when the robot walks in a straight pipe, its motion characteristics obey the following rules:

(1) The deflection angle of each driving wheel must be kept the same.

(2) Because the deflection angle of the driving wheel is generally between 0° and 90°, the tangent value of the deflection angle is always a positive value. Thus, the velocity of the robot motion is only related to the velocity of the drive frame, i.e., it is related to the forward and reverse rotation of the motor.

(3) The speed is related to the rotation speed of the drive frame and the deflection angle of the drive wheel, which is tangentially proportional to the deflection angle of the drive wheel and proportional to the rotation speed of the drive frame (motor speed).

Integrating Equation (12) over time and replacing it with Equation (5) yields the following:

$$ {}^0P = \begin{bmatrix} -R\sin\alpha \\ R\cos\alpha \\ R\alpha\tan\theta \end{bmatrix} \tag{13} $$

Using Equation (13), the walking trajectory equation of the robot in the straight pipe can be obtained, and the walking trajectory of the robot is shown in Figure 11 (the diameter of the pipe was set to 200 mm and the deflection angle of the driving wheel was set to 25 °).

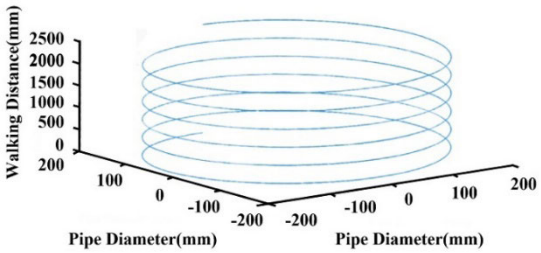

FIGURE 11. Driving trajectory of wheel I in a straight pipe.

B. ANALYSIS OF MOTION CHARACTERISTICS OF PLUGGING ROBOT INSIDE BENT PIPE

Elbow joints are the main connection component for turns when laying oil and gas pipelines, and they are also unavoidable obstacles during the driving process of a sealing robot in a pipeline. This paper mainly examines the passing performance of the robot in a curved pipe with a 500 mm radius of curvature.

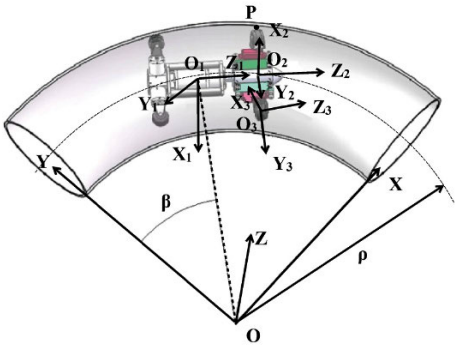

FIGURE 12. Schematic diagram of the robot driving in a curved pipe.

The driving process of the robot in the curved pipe is shown in Figure 12. The parameters used are basically the same as those described above. The radius of curvature of the curved pipe was set to ρ.

To study the motion state of the robot in the curved pipe, a coordinate system is established in Figure 12. $\{O\}$ is the global coordinate system established on the ground, and its origin is the center of curvature of the bend. During the turning process, the robot rotates around the Z axis in $\{O\}$. $\{O_1\}$ is the dynamic coordinate system of the geometric center of the robot, whose origin can be expressed as (ρ sin $\beta\rho\cos\beta$ 0) in $\{O\}$, and β is the steering angle of the robot. $\{O_2\}$ is the dynamic coordinate system on the drive frame. Its origin is at the intersection of the plane formed by the central axis of the robot and the centerline of the output shafts of the three servos in the drive frame. It is represented as $(0\ 0\ z)^T$ in $\{O_1\}$. The Z_2 axis coincides with the Z_1 axis of $\{O_1\}$, and the Y_2 axis coincides with the centerline of the rotation axis of the servo. The X_2Y_2 plane of $\{O_2\}$ rotates around the Z_1 axis of $\{O_1\}$, and the rotation angle is α, where α ' can represent the drive speed of the rack. $\{O_3\}$ is the dynamic coordinate system on the center of the driving wheel, and its origin can be expressed as $(0\ y\ 0)^T$ in $\{O_2\}$, whose Y_3 axis coincides with the Y_2 axis in $\{O_2\}$. The Y_2 axis deflection angle in $\{O_2\}$ is θ (the deflection angle of the drive wheel set by the robot when turning).

The transformation between different coordinate systems is described in the form of a matrix, which is described as follows:

$$ {}^{0}_{1}T = \begin{bmatrix} \cos\beta & -\sin\beta & 0 & \rho\sin\beta \\ \sin\beta & \cos\beta & 0 & \rho\cos\beta \\ 0 & 0 & 1 & 0 \\ 0 & 0 & 0 & 1 \end{bmatrix} \tag{14} $$

$$ {}^{1}_{2}T = \begin{bmatrix} \cos\alpha & -\sin\alpha & 0 & 0 \\ \sin\alpha & \cos\alpha & 0 & 0 \\ 0 & 0 & 1 & z \\ 0 & 0 & 0 & 1 \end{bmatrix} \tag{15} $$

$$ {}^{2}_{3}T = \begin{bmatrix} \cos\theta & 0 & \sin\theta & 0 \\ 0 & 1 & 0 & y \\ -\sin\theta & 0 & \cos\theta & 0 \\ 0 & 0 & 0 & 1 \end{bmatrix} \tag{16} $$

It is assumed that each of the driving wheels is in contact with the tube wall during the driving process, and the contact form is point contact. The contact point between the driving wheel and the inner wall of the tube is denoted as **P**, and the point **P** in $\{O_3\}$ is expressed as follows:

$$ {}^{3}P = (0 \quad r \quad 0)^T \tag{17} $$

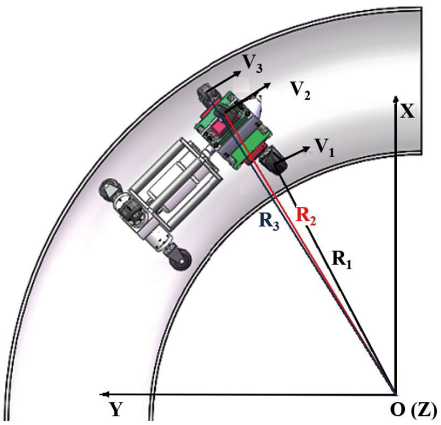

FIGURE 13. Mechanical analysis of the robot through the curved pipe.

The following is a qualitative analysis of the robot's turning characteristics from the perspective of analytic geometry. The movement of each drive wheel during the robot's turning process is shown in Figure 13, as shown in the mechanical analysis diagram when the robot passes through the bend. The curvature center of the bend is not in the plane where the centerline of the output rotation axis of the three drive wheels of the robot is located, indicating that the contact condition of each wheel and the bend is inconsistent during the robot's turning process. In addition, the robot's turning diagram shows that the driving wheels rotate at different

speeds around the z-axis of the global coordinate system. In the turning stroke of the inner blocking robot, the bending speed components of each driving wheel have the following relationship:

$$v_1 : v_2 : v_3 = R_1 : R_2 : R_3 \tag{18}$$

R_1, R_2, and R_3 are constantly changing during the turning of the robot, and $R_1 \neq R_2 \neq R_3$. Thus, the speeds of the driving wheels of the robot during turning are not equal, and the driving speeds of the driving wheels near the center of curvature of the curved pipe are slow.

According to the above analysis, the movement characteristics of the robot during the turning process obey the following rules:

(1) The speed of each driving wheel is different. The speed near the inside of the curved pipe is smaller than the outside speed, and the speed of each driving wheel undergoes the same periodic variation.

(2) In the process of turning, the robot needs to ensure that each wheel contacts the inner wall of the pipeline at the same time to prevent slipping as much as possible. This requires each wheel to have a certain adaptive ability.

The specific process of each turn is different, but the characteristics are the same throughout the turn. The driving wheel is the entry point for each process. It is assumed that the driving wheel is always in contact with the inner wall of the elbow during the turning process, and the contact point is denoted as **P**. The representation of point **P** in {O} is as follows:

$$P = \begin{bmatrix} (\rho + R\cos\alpha)\cos\dfrac{R\alpha\tan\theta}{\rho} \\ (\rho + R\cos\alpha)\sin\dfrac{R\alpha\tan\theta}{\rho} \\ R\sin\alpha \end{bmatrix} \tag{19}$$

where ρ is the radius of curvature of the curved pipe, $\boldsymbol{R}$ is the inner radius of the pipeline, α is the corner of the drive frame, and θ is the deflection angle of the drive wheel.

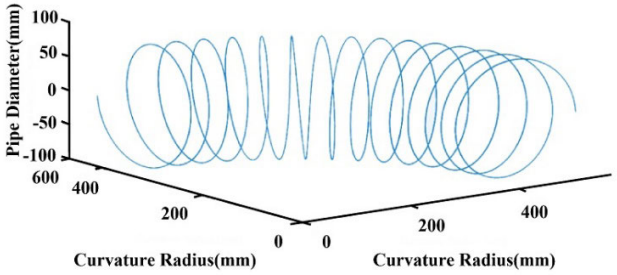

FIGURE 14. Walking path of driving wheel I during the turn.

Using Equation (19), the walking path equation of the robot in the elbow can be obtained, an example path is shown in Figure 14 (the diameter of the pipe was set as 200 mm, the radius of curvature was 500 mm, and the deflection angle of the driving wheel was 25°).

Through the analysis of the two main motion states of the pipeline robot, it was found that the factors affecting its passing performance are the deflection angle of the driving wheel and the rotation speed of the driving frame. The speed of the driving frame can be controlled by the motor, and the deflection angle of the driving wheel is controlled by the servo steering gear.

IV. IN-PIPE PLUGGING ROBOT ANALYSIS

A. ESTABLISHMENT OF SIMULATION MODEL AND PARAMETER SETTING

The simulation analysis of the plugging robot in the pipeline was mainly performed using virtual prototype technology to simulate and measure the performance indicators and evaluate the rationality of the robot model design [34].

A three-dimensional model of the robot was built using the Solidworks software. To shorten the simulation time and reduce the interactions of the various components in the simulation software, the motor unit and the rear support frame were integrated as a single part. Furthermore, the steering gear, steering gear cover, and wheel frame of the driving wheel were integrated, and the rear support arm and the wheel frame supporting the wheel were integrated. The established model was exported and imported into ADAMS, and the motion pairs between each part were added.

First, a fixed constraint between the pipeline and the ground was added, a mobile pair between the servo unit and the drive frame was added, and a mobile pair between the support arm and the support frame was added. A rotation constraint was added between each wheel and the wheel frame, and a rotation pair was added between the drive frame and the motor. Second, based on the set position of the spring when the robot drive unit was designed, a spring was added to the simulation model. Finally, the contact constraints of the driving wheels, support wheels, and pipe wall were added. In the simulation, the friction coefficient between each wheel and the pipe wall was set to 0.8, the rotation speed of the motor was 30 r/min, and the inner diameter of the pipe was set to 200 mm. The simulation software automatically calculated the addition. No medium was added inside the pipe, and the pipe was surrounded by air for this study. Figure 15 shows the completed robot drive unit model.

B. CLIMBING PERFORMANCE ANALYSIS OF PLUGGING ROBOT IN PIPELINE

One of the most common obstacles is a slope obstacle when the robot is operating in a pipeline.

1) FORCE ANALYSIS

The driving part of the robot drive unit provides power for the entire system, and the study of the climbing performance of the entire system was simplified to the study of the climbing performance of the robot drive unit. The driving diagram of the robot drive unit during the climbing process is shown in Figure 16. It was assumed that all the wheels of the robot

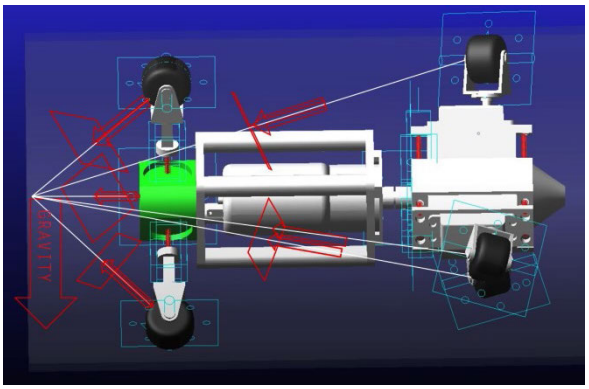

FIGURE 15. Simulation model of the robot drive unit.

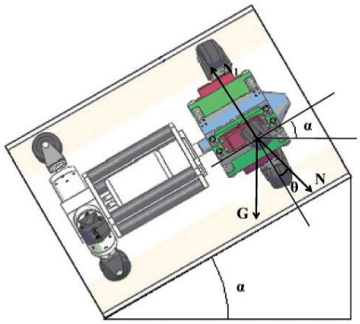

FIGURE 16. Schematic diagram of the climbing process of the robot drive unit.

drive unit were in contact with the inner wall of the pipeline, and the force analysis of its driving wheels was performed.

Analysis of the forces on the front wheels showed that when the robot is climbing a hill, the front drive wheels are affected by gravity, the support, and the driving forces. The three driving wheel frames of the robot are arranged in a circular array of 120°. The driving force received by each driving wheel is one third of the motor torque, expressed as follows:

$$N = \frac{Tw}{3R} \tag{20}$$

where $\boldsymbol{Tw}$ is the torque of the motor, $\boldsymbol{R}$ is the radius of the pipe, and $\boldsymbol{N}$ is the driving force of the single driving wheel.

The force of gravity acting on a single driving wheel is related to the robot's posture. Ignoring the influence of the attitude, it is assumed that the weight supported by a single driving wheel is one half of the robot's weight, expressed as follows:

$$G = \frac{Mg}{2} \tag{21}$$

where $\boldsymbol{M}$ is the mass of the robot, $\boldsymbol{g}$ is the acceleration due to gravity, and $\boldsymbol{G}$ is the gravitational force acting on a single drive wheel.

The traction force of the robot when climbing the inclined pipe is expressed as follows:

$$F = N\sin\theta - G\sin\alpha \tag{22}$$

where θ is the deflection angle of the drive wheel, and α is the angle of the slope.

For the robot to climb the inclined pipe smoothly, $F \geq 0$ must be satisfied. Thus, the sufficient condition for the robot to climb the inclined pipe is $N{\cdot}\sin\theta \geq G{\cdot}\sin\alpha$.

During the climbing of the robot, the robot will also slip due to insufficient static friction between the driving wheels and the tube wall, which will cause the robot to slide. Therefore, another sufficient condition for the robot to climb up the inclined pipe is $f \geq N{\cdot}\sin\alpha$.

2) SELECTION OF SPRING STIFFNESS

As discussed above, the robot torque and static friction force play key roles in the climbing process of the robot. The motor model was determined. The static friction between the driving wheels and the tube wall is not only related to the quality of the robot and the material of the wheel but also to the selection of the spring stiffness in the design of the robot. The selected springs are shown in Table 3.

TABLE 3. Selected spring specifications.

Diameter (mm)	Outer diameter (mm)	Length (mm)
0.8	8	20
1.0	8	20
1.2	9	20
1.4	9	20

The spring stiffness is calculated as follows:

$$K = \frac{Gd^4}{8D^3n} \tag{23}$$

where: $\boldsymbol{K}$ is the spring stiffness, $\boldsymbol{G}$ is the elastic modulus of the spring (generally 79,000 *MPa*), $\boldsymbol{d}$ is the diameter of the spring wire, $\boldsymbol{D}$ is the diameter of the spring, and $\boldsymbol{n}$ is the effective number of turns of the spring.

Based on the design requirements of the robot, the spring stiffness values were selected to be 2, 5, 9, 13, and 17 N/mm. The robot was designed to climb an inclined pipe with a slope of 30°, so the simulation environment was set to a slope of 30°. The driving wheel deflection angle of the robot was set to 25°, and the other parameters were consistent with those described above. (based on the previous simulations, when the deflection angle of the driving wheel was set to 25° ∼ 40°, the robot could operate smoothly and stably in the straight tube; we mainly explore the influence of spring stiffness on the climbing performance of the robot below.)

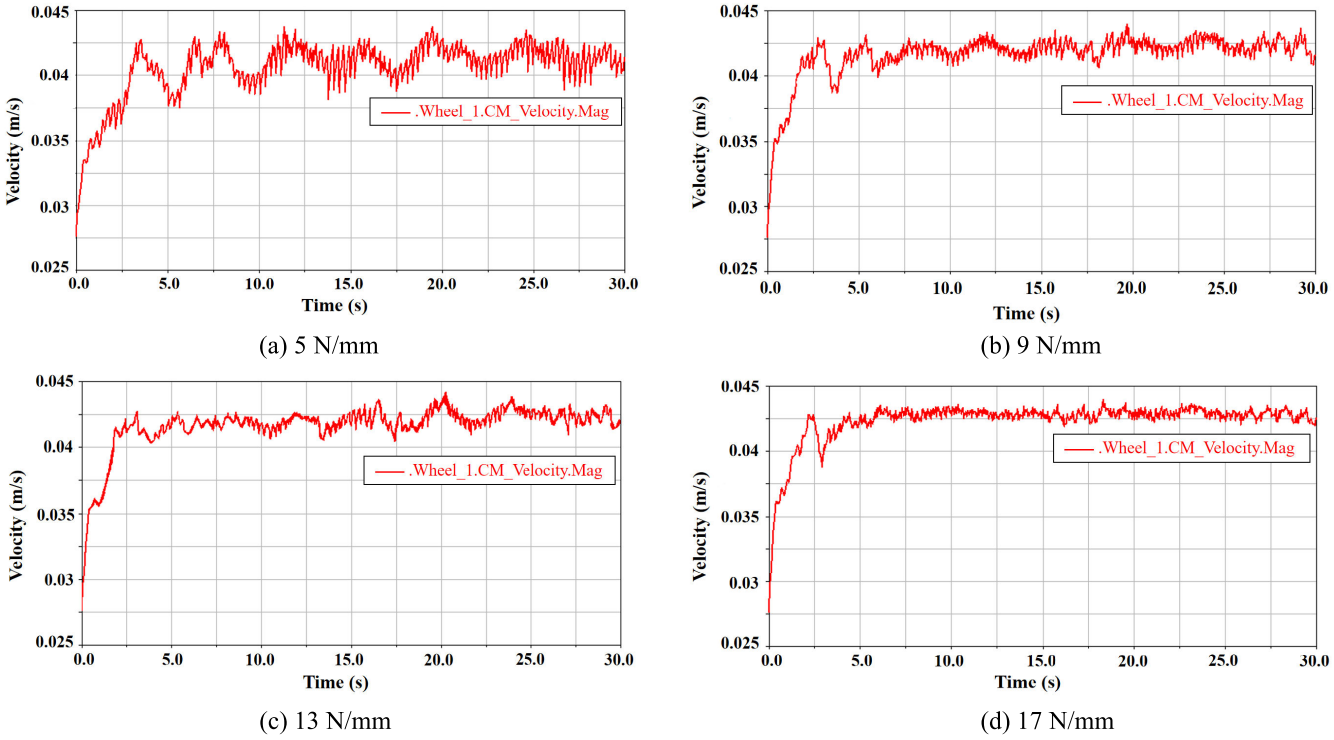

FIGURE 17. Speed changes of driving wheel I with different spring stiffness values.

3) IMPACT OF SPRING STIFFNESS ON CLIMBING PERFORMANCE OF ROBOT

When the spring stiffness of the robot drive unit was set to 2 N/mm, the robot slid along the pipe wall under the action of gravity. Thus, a spring with a stiffness of 2 N/mm was insufficient to support the robot to complete the climbing and driving process. Figure 17 shows the speed change of driving wheel I when the robot drive unit climbed the inclined pipe for different spring stiffness values.

A comparison showed that when the stiffness was 5 N/mm, the running speed of the driving wheel varied greatly. When the stiffness was 9 N/mm, the change in the speed of the drive wheel was significantly smaller than that when the spring stiffness was 5 N/mm, and the speed change interval was within the normal jitter range of the robot. When the spring stiffness was 13 N/mm, the walking speed of the drive wheel was more stable than that when the spring stiffness was 9 N/mm, but there was still a slight jitter phenomenon. When the spring stiffness was 17 N/mm, the operating speed of the driving wheel varied little, and the running was relatively stable, making this the ideal spring stiffness. This analysis showed that when the robot climbs a pipe with a slope of 30°, it is possible to choose a spring with a stiffness value of 9, 13, and 17 N/mm, or the body runs more smoothly when the stiffness is greater.

The ADAMS simulation analysis was used to determine the required output torque of the motor, and the results are shown in Table 4. When the stiffness was 17 N/mm, the required motor output torque was 4.5 N·m, which exceeded the rated torque of the motor selected previously. In summary, a spring with a stiffness of 9 or 13 N/mm should be selected when climbing a 30° inclined pipe.

TABLE 4. Motor output torque corresponding to different spring stiffness.

Spring stiffness (N/mm)	Torque (N·m)
9	2.5
13	3.3
17	4.5

C. ANALYSIS OF PASSING PERFORMANCE OF ROBOT IN PIPE

Pipe bends are connection pipes in oil and gas pipeline networks. A robot's ability to pass through bends is also one of its important technical indicators. Based on the design requirements, the research objective was to study the rationality of the structural dimension design of the robot and the influence of the deflection angle of the driving wheel on the cornering characteristics of the robot in a 500-mm curved pipe as the research goal.

a: PASSING ABILITY SIMULATION ANALYSIS

The turning process of the robot drive unit in ADAMS is shown in Figure 18. During the operation, the drive frame

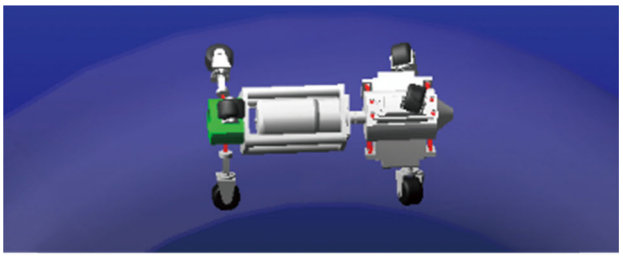

FIGURE 18. Schematic diagram of the turning process of the robot drive unit.

drives the front drive mechanism to rotate, and the robot moves forward by relying on the friction between the drive wheel and tube wall. The rear support wheel contacts the tube wall to support it. As evident, there was no interference problem between the robot drive unit and the pipe wall when the robot was running, and it smoothly passed the pipe bend. Therefore, the structural size of the robot was determined to meet the requirements.

b: ANALYSIS OF INFLUENCE OF DIFFERENT DEFLECTION ANGLES OF DRIVING WHEELS ON CORNERING SPEED OF ROBOT

In the cornering simulation analysis, only the deflection angle of the driving wheels of the robot changed, and the other settings were consistent with those described above (the spring rigidity was set to 9 N/mm). Early simulations were conducted. For the robot to meet its driving requirements, the deflection angle of the drive wheel should be set between 25° and 40°. The driving wheel deflection angles examined were 25°, 30°, 35°, and 40°. For a deflection angle of the driving wheels of 25° ($\theta = 25°$), the cornering speeds of each driving wheel obtained through the simulations are shown in Figure 19.

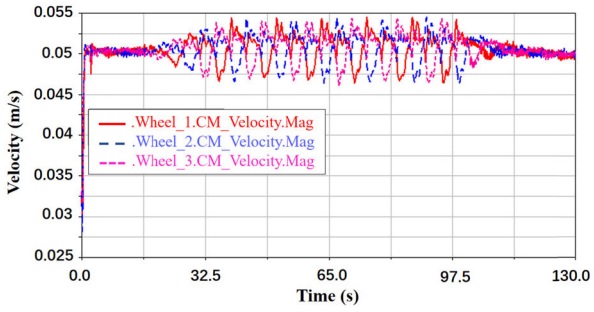

FIGURE 19. Turning speed of each driving wheel at $\theta = 25$ °.

Figure 19 shows that during the turning of the robot drive unit, the walking speed of each driving wheel was divided into two parts: a driving part in the straight pipe and a turning part in the bent pipe.

(1) In the 0–20 s and 110–130 s ranges, the robot was in the driving part in the straight pipe. The driving speeds of each driving wheel were basically the same. This verified the conclusion that the driving speeds of each driving wheel are equal when the robot described above is driving in a straight pipe.

(2) In the 20–110 s range, the robot was in the process of turning, the driving speeds of each driving wheel were different, and there were periodic changes. The driving wheel's cornering speed variations were basically the same, which indicated that during the robot's turning process, the driving wheel's cornering attitude was constantly changing, but the motion cycles of different driving wheels were the same.

The change in the driving speed of a single driving wheel was analyzed. Taking driving wheel I as an example, the change in the cornering speed is shown in Figure 20.

When the drive wheel deflection angle was 25°, the robot exhibited significant fluctuations at the maximum speed when turning. The simulation animation of the driving wheel I showed that the driving wheel was at the outer side of the pipe at the maximum speed, which indicated that the robot ran unstably outside the pipe. When the deflection angles of the driving wheels were 35° and 40°, the speed of the robot changed greatly during the cornering process, which indicated that its body movement was more unstable during the turning process. When the deflection angle of the driving wheel was 30°, compared with 35° and 40°, the speed varied relatively gently, indicating that the robot underwent smoother cornering.

During the turn of the plugging robot in the pipeline, a driving wheel deflection angle of 30° was finally selected.

V. EXPERIMENTAL STUDY ON PLUGGING ROBOTS IN PIPELINES

Based on the design requirements, a prototype model was constructed, and an experimental platform was established to complete the determination of the robot design indicators and verify the reliability of the simulation results.

A. CONSTRUCTION OF EXPERIMENTAL PROTOTYPE AND PLATFORM

1) EXPERIMENTAL PROTOTYPE ASSEMBLY

Based on the design requirements, a model of the plugging robot was drawn, processed, and assembled, as shown in Figure 21. The prototype model was basically the same as the theoretical model simulated above. The sealing airbag was replaced by rubber tires in the plugging unit. The total length of the plugging robot drive unit in the pipeline was 580 mm, and the total weight was 6.4 kg, which met the design requirements.

2) CONSTRUCTION OF EXPERIMENTAL PLATFORM

Following the experimental design requirements, an experimental platform was constructed, as shown in Figure 22. The platform mainly included three components: the pipeline plugging robot, the control system, and the pipeline system. The robot was required to complete cornering and climbing tests. The control system was required to control the motor's

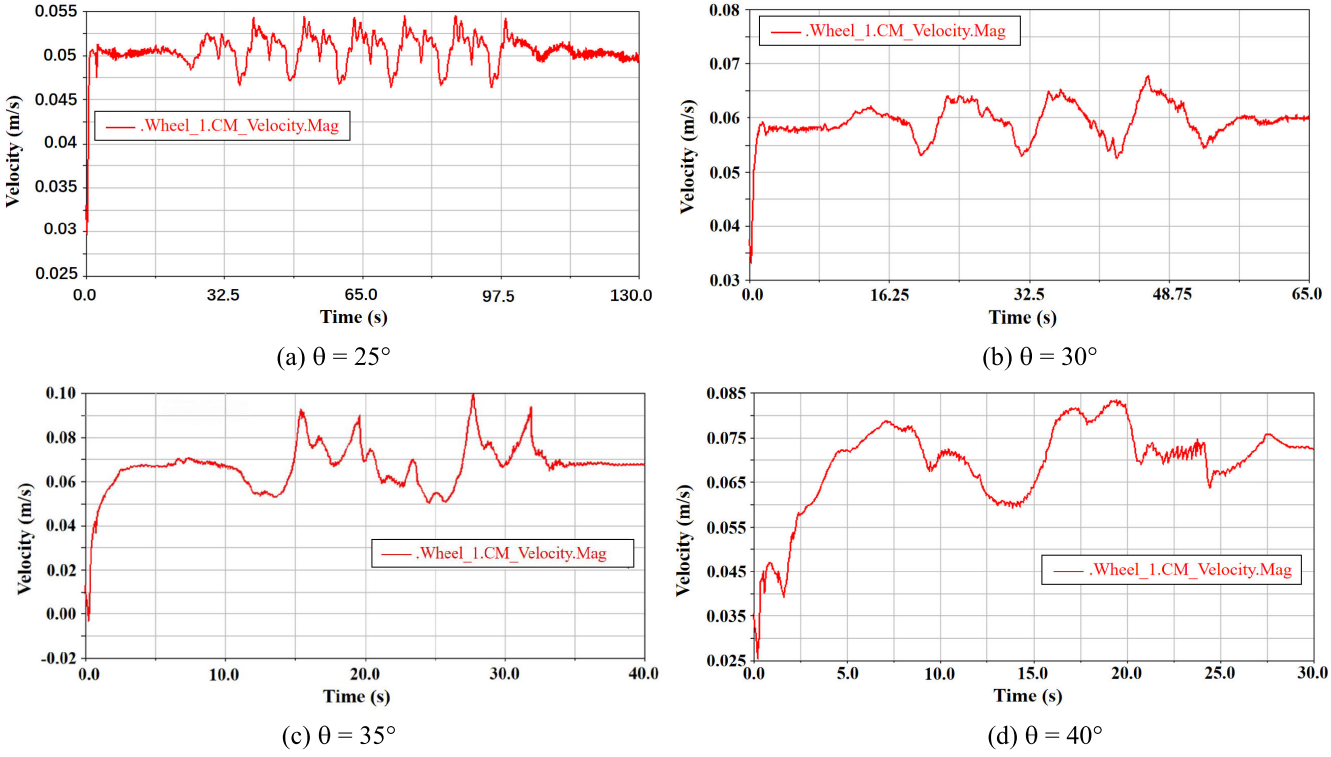

FIGURE 20. Turning speeds of drive wheel I at $\theta = 25°$, 30°, 35°, and 40°.

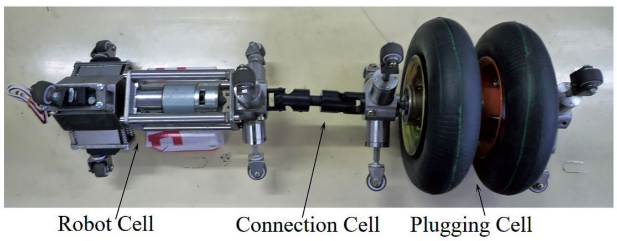

FIGURE 21. Experimental prototype of a plugging robot for a pipeline.

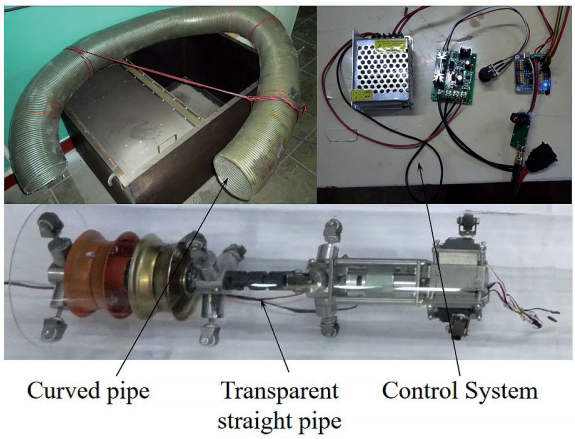

FIGURE 22. Experimental platform.

FIGURE 23. Photographs of the robot climbing the inclined pipe.

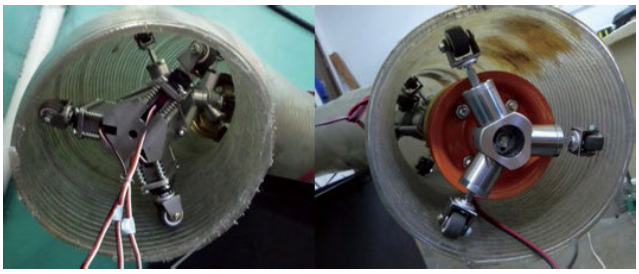

FIGURE 24. Photograph of cornering robot in pipeline.

forward and reverse rotation and the motor speed. The piping system mainly included a 1.5 m plexiglass transparent straight pipe with an inner diameter of 200 mm, and a steel wire curved pipe with an inner diameter of 200 mm and a bending radius of 500 mm. The climbing performance experiment of the robot was completed in a transparent straight pipe, and the bendability test of the robot was completed in a wire pipe bend. In the experiment, the pipe was placed in the air, and no medium was added in the pipe.

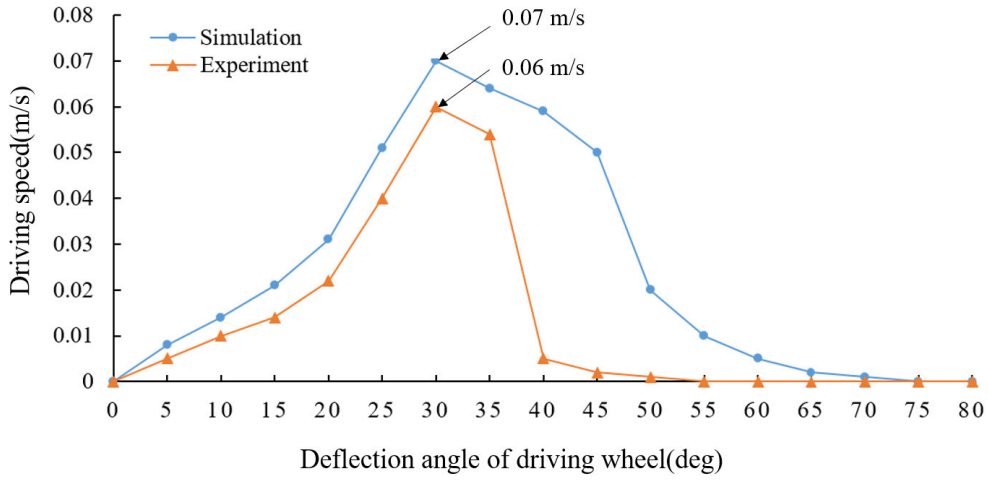

FIGURE 25. Test environment for running speed of test prototype.

B. EXPERIMENTAL TEST OF PLUGGING ROBOT IN PIPELINE

1) CLIMBING PERFORMANCE TEST

The transparent straight tube was inclined with an angle of 30°, the rotation speed of the robot motor was set to 30 r/min, and the deflection angle of the driving wheel was 25°. The climbing performances of the robot with spring stiffness values of 5, 9, 13, and 17 N/mm were studied.

The climbing process of the robot is shown in Figure 23. When the spring stiffness was 5 N/mm, the robot could climb a tube with up to a 30° incline, but when the motor stopped running, the robot slid down the inclined tube, indicating that the spring stiffness was not sufficient to hold the robot in place. When the spring stiffness values were 9 and 13 N/mm, the robot could smoothly climb a 30° inclined pipe and continued to climb the straight pipe up to an angle of 37°. Both types of springs allowed the robot to stay in the pipe stably. When the stiffness was 13 N/mm, the robot ran more smoothly. When a spring stiffness of 17 N/mm was selected, the robot became stuck and could not move normally. Therefore, when climbing the oblique pipe inside the pipeline, the optimal rigidity should be approximately 13 N/mm due to the influence of external factors, such as friction, as summarized in Table 5.

TABLE 5. Results of climbing experiment.

Spring rate	5 N/mm	9 N/mm	13 N/mm	17 N/mm
Whethe robot completed climbing process	Yes	Yes	Yes	No
Climbing angle	30°	37°	37°	—
Stability	Driving stopped and robot slipped	Steady speed	Compared with rigidity of 9 N/mm, robot ran more smoothly at this speed.	Stuck

2) BENT PIPE PASSING ABILITY TEST

This experiment mainly tested the passing performance of the robot in a known elbow. The elbow shown in Figure 24 was a steel wire bellows. Based on the design requirements, the bending radius of bellows is 500mm and placed in a certain slope environment. Compared with other pipes, the unsmooth characteristics of the steel corrugated pipe highlight the superior performance of the designed pipeline blocking robot when turning.

Over the course of the experiment, the speed of the motor was set to 30 r/min, and the deflection angles of the driving wheels of the robot were set to 25°, 30°, 35°, and 40°. The cornering characteristics of the robot at different deflection angles were studied. The experimental process is shown in Figure 24.

Figure 25 shows that the running speed of the sample through the elbow was approximately the same as the simulation result, but the overall experimental result was smaller. The maximum value of the simulation result was 0.07 m/s, and the maximum value of the experimental result was 0.06 m/s. The results showed that the speed of the prototype wheel increased with the increase in the deflection angle of

the driving wheel between 0° and 30°, and the speed of the prototype wheel peaked at 30°. The robot could successfully pass the bent pipe in the experiment, and had a good barrier-crossing ability and bent pipe passing ability. The overall speed of the prototype was lower than the simulated speed, because in the simulation, the perfect fit of each part of the prototype was not guaranteed, and a slip phenomenon occurred between the drive wheels and the tube wall.

When the spiral drive angle continued to increase to 40°, a relatively significant slip phenomenon began to occur at a low motor speed, and the joint between the straight pipes in the elbow could not be crossed. The obstacle resistance of the robot deteriorated, and the motor continued to increase. When the speed reached 30% of the maximum speed, the robot's ability to overcome obstacles was improved, and the test elbow was passed. The results were similar when the spiral drive angles were 45° and 50°.

When the screw drive angle continued to increase to 55°, the pipeline robot was not able to operate normally in the test elbow, and the spindle motor speed did not reach the maximum value.

VI. CONCLUSION

In this paper, a robot for the internal plugging of the pipes was designed independently, and its climbing and pipe bend passing performances were simulated and analyzed. The following conclusions were drawn:

(1) The overall size and weight of the plugging robot in the pipeline met the design requirements, and the robot could operate normally, confirming the rationality of its structural design.

(2) A spring with a stiffness of 13 N/mm should be selected to achieve the best climbing performance of the plugging robot in the pipeline, allowing it to climb straight pipes with slopes up 37°.

(3) When the deflection angle of the driving wheel was set to 30°, the plugging robot could smoothly pass through the bend with a radius of curvature of 500 mm.

DECLARATION

ACKNOWLEDGMENT

The authors would like to express their gratitude for the support of this study. The authors thank LetPub (www.letpub.com) for its linguistic assistance during the preparation of this manuscript.

AUTHOR CONTRIBUTIONS

The author contributions were as follows. Hongwei Yan wrote the manuscript and integrated the modification suggestions of the other authors. Lu Wang and Xiong Yang built the three-dimensional model of the robot, and completed the simulations and experiments of the robot. Pengcheng Li and Zhijian Wang were responsible for analyzing the simulation and experimental data, and writing summary reports. Xiangrong Hou was responsible for the construction of the experimental platform and the purchase of related equipment.

COMPETING INTERESTS

The authors declare no competing financial interests.

REFERENCES

[1] B. Liu, S. Liu, S. Guo, and S. Zhang, "Economic study of a large-scale renewable hydrogen application utilizing surplus renewable energy and natural gas pipeline transportation in China," *Int. J. Hydrogen Energy*, vol. 45, no. 3, pp. 1385–1398, Jan. 2020.

[2] H. Xu, B. Bbosa, E. Pereyra, M. Volk, and M. S. Mannan, "Oil transportation in pipelines with the existence of ice," *J. Loss Prevention Process Ind.*, vol. 56, pp. 137–146, Nov. 2018.

[3] Q. H. Tian, "Robust and stepwise optimization design for CO_2 pipeline transportation," *Int. J. Greenhouse Gas Control*, vol. 58, pp. 10–18, Mar. 2017.

[4] R. Adiputra and T. Utsunomiya, "Stability based approach to design cold-water pipe (CWP) for ocean thermal energy conversion (OTEC)," *Appl. Ocean Res.*, vol. 92, Nov. 2019, Art. no. 101921.

[5] N. A. Barton, T. S. Farewell, S. H. Hallett, and T. F. Acland, "Improving pipe failure predictions: Factors affecting pipe failure in drinking water networks," *Water Res.*, vol. 164, Nov. 2019, Art. no. 114926.

[6] Y. Gong and Y. Li, "STAMP-based causal analysis of China-donghuang oil transportation pipeline leakage and explosion accident," *J. Loss Prevention Process Industries*, vol. 56, pp. 402–413, Nov. 2018.

[7] T. Bui Quy and J.-M. Kim, "Leak detection in a gas pipeline using spectral portrait of acoustic emission signals," *Measurement*, vol. 152, Feb. 2020, Art. no. 107403.

[8] A. G. D. Almeida and J. E. Vinnem, "Major accident prevention illustrated by hydrocarbon leak case studies: A comparison between brazilian and norwegian offshore functional petroleum safety regulatory approaches," *Saf. Sci.*, vol. 121, pp. 652–665, Jan. 2020.

[9] S. Yang, K. Jeon, D. Kang, and C. Han, "Accident analysis of the gumi hydrogen fluoride gas leak using CFD and comparison with post-accidental environmental impacts," *J. Loss Prevention Process Ind.*, vol. 48, pp. 207–215, Jul. 2017.

[10] H. Li, R. Li, J. Zhang, and P. Zhang, "Development of a pipeline inspection robot for the standard oil pipeline of China national petroleum corporation," *Appl. Sci.*, vol. 10, no. 8, p. 2853, Apr. 2020.

[11] H. Lu, X. Wu, H. Ni, M. Azimi, X. Yan, and Y. Niu, "Stress analysis of urban gas pipeline repaired by inserted hose lining method," *Compos. B, Eng.*, vol. 183, Feb. 2020, Art. no. 107657.

[12] A. Kakogawa and S. Ma, "Design of a multilink-articulated wheeled pipeline inspection robot using only passive elastic joints," *Adv. Robot.*, vol. 32, no. 1, pp. 25–37, 2017.

[13] A. V. S. Bhadoriya, V. K. Gupta, and S. Mukherjee, "Development of in-pipe inspection robot," *Mater. Today, Proc.*, vol. 5, no. 9, pp. 20769–20776, 2018.

[14] A. V. Reyes-Acosta, I. Lopez-Juarez, R. Osorio-Comparan, and G. Lefranc, "3D pipe reconstruction employing video information from mobile robots," *Appl. Soft Comput.*, vol. 75, pp. 562–574, Feb. 2019.

[15] H. Zhang, J. Dong, C. Cui, and S. Liu, "Stress and strain analysis of spherical sealing cups of fluid-driven pipeline robot in dented oil and gas pipeline," *Eng. Failure Anal.*, vol. 108, Jan. 2020, Art. no. 104294.

[16] M. H. W. Hendrix, H. P. Ijsseldijk, W.-P. Breugem, and R. A. W. M. Henkes, "Experiments and modeling of by-pass pigging under low-pressure conditions," *J. Process Control*, vol. 71, pp. 1–13, Nov. 2018.

[17] M. H. Sadeghi, S. Chitsaz, and M. M. Ettefagh, "Effect of PIG's physical parameters on dynamic behavior of above ground pipeline in pigging operation," *Mech. Syst. Signal Process.*, vol. 132, pp. 692–720, Oct. 2019.

[18] C. Liu, Y. Wei, Y. Cao, S. Zhang, and Y. Sun, "Traveling ability of pipeline inspection gauge (PIG) in elbow under different friction coefficients by 3D FEM," *J. Natural Gas Sci. Eng.*, vol. 75, Mar. 2020, Art. no. 103134.

[19] H. M. Kim, Y. S. Choi, Y. G. Lee, and H. R. Choi, "Novel mechanism for in-pipe robot based on a multiaxial differential gear mechanism," *IEEE/ASME Trans. Mechatronics*, vol. 22, no. 1, pp. 227–235, Feb. 2017.

[20] J. Nagase, F. Fukunaga, and K. Ishida, "Steering system of cylindrical elastic crawler robot," *IEEJ J. Ind. Appl.*, vol. 7, no. 5, pp. 441–442, 2018.

[21] T. Ito, H. Kono, Y. Tamura, A. Yamashita, H. Asama, "Recovery motion learning for arm mounted mobile crawler robot in drive system's failure," *IFAC-Papers Online*, vol. 50, no. 1, pp. 2329–2334, 2017.

[22] A. Bonato, R. M. del Río-Chanona, C. MacRury, J. Nicolaidis, X. Pérez-Giménez, P. Praáat, and K. Ternovsky, "The robot crawler graph process," *Discrete Appl. Math.*, vol. 247, pp. 23–36, Oct. 2018.

[23] Y. Cao, S. Suzuki, and Y. Hoshino, "Uphill and level walking of a three-dimensional biped quasi-passive walking robot by torso control," *Robotica*, vol. 34, no. 3, pp. 483–496, Mar. 2016.
[24] Y. Mano, R. Ishikawa, and Y. Yamada, "Development of contraction force control system of peristaltic crawling robot for sewer pipe inspection," in *Proc. IEEE/ASME Int. Conf. Adv. Intell. Mechatronics*, 2018, pp. 936–941.
[25] M. Manjunatha and A. Selvakumar, "A low cost underwater robot with grippers for visual inspection of external pipeline surface," *Procedia Comput. Sci.*, vol. 133, pp. 108–155, Jan. 2018.
[26] C. Z. Ferreira, R. Cardoso, M. E. M. Meza, and J. P. J. Ávila, "Controlling tracking trajectory of a robotic vehicle for inspection of underwater structures," *Ocean Eng.*, vol. 149, pp. 373–382, Feb. 2018.
[27] M. Kamata, S. Yamazaki, and Y. Tanise, "Development of pneumatically driven peristaltic-type robot for long distance inspection in half-inch pipes," in *Proc. IEEE/ASME Int. Conf. Adv. Intell. Mechatronics*, Jul. 2017, pp. 309–314.
[28] P. Bhovad, J. Kaufmann, and S. Li, "Peristaltic locomotion without digital controllers: Exploiting multi-stability in origami to coordinate robotic motion," *Extreme Mech. Lett.*, vol. 32, Oct. 2019, Art. no. 100552.
[29] A. Kakogawa and S. Ma, "Stiffness design of springs for a screw drive in-pipe robot to pass through curved pipes and vertical straight pipes," *Adv. Robot.*, vol. 26, nos. 3–4, pp. 253–276, Jan. 2012.
[30] A. Kakogawa, T. Nishimura, and S. Ma, "Designing arm length of a screw drive in-pipe robot for climbing vertically positioned bent pipes," *Robotica*, vol. 34, no. 2, pp. 306–327, Feb. 2016.
[31] D. Xia, X. Chen, Y. Tian, C. Liu, and Z. Wang, "Design of polarizers with smooth grooves by the coordinate transformation method for ECH&CD system," *Fusion Eng. Des.*, vol. 139, pp. 137–141, Feb. 2019.
[32] H. H. Sidhwa, R. P. R. C. Aiyar, and Z. Kavehvash, "Cloaking of irregularly shaped bodies using coordinate transformation," *Optik*, vol. 197, Nov. 2019, Art. no. 163201.
[33] W. Rydlewicz, M. Rydlewicz, and T. Paáczyáski, "Experimental investigation of the influence of an orifice plate on the pressure pulsation amplitude in the pulsating flow in a straight pipe," *Mech. Syst. Signal Process.*, vol. 117, pp. 634–652, Feb. 2019.
[34] J. He, Q. Zhou, J. Guo, J. Gao, and F. Fang, "Incredulity on assumptions for the simplified bohart-adams model: 17a-ethinylestradiol separation in lab-scale anthracite columns," *J. Hazardous Mater.*, vol. 384, Feb. 2020, Art. no. 121501.

HONGWEI YAN was born in Taiyuan, Shanxi, China. He received the Ph.D. degree in mechanical engineering from the Taiyuan University of Technology. He is currently an Associate Professor and a master's Supervisor with the School of Mechanical Engineering, North University of China. His main research interests include dangerous emergency equipment, and prevention and control technology.

LU WANG was born in Shanxi, China. She received the bachelor's degree in process equipment and control engineering from the North University of China, in 2018, where she is currently pursuing the master's degree in mechanical engineering. Her main research interests include pipeline robots and machinery manufacturing automation.

PENGCHENG LI was born in Shanxi, China. He received the bachelor's degree in process equipment and control engineering from the North University of China, in 2018, where he is currently pursuing the master's degree in mechanical engineering. His main research interest includes mechatronics.

ZHIJIAN WANG received the Ph.D. degree from the Taiyuan University of Technology, Taiyuan, China. He is currently an Associate Professor with the North University of China. He has published more than 12 articles in these fields. His research interests include mechanical fault diagnosis, signal processing, and intelligent diagnosis. He is a member of the Chinese Society of Vibration Engineering.

XIONG YANG was born in Shanxi, China. He received the bachelor's degree in mechanical design manufacture and automation from the North University of China, in 2018, where he is currently pursuing the master's degree in mechanical engineering. His main research interests include pipeline robots and machinery manufacturing automation.

XIANGRONG HOU was born in Shanxi, China. He received the bachelor's degree in mechanical design manufacture and automation from the North University of China, in 2016, where he is currently pursuing the master's degree in mechanical engineering. His main research interest includes mechanical design theory.